Mass Transport Across Droplet Interfaces by Atomistic Simulations

Matthias Heinen, Simon Homes, Gabriela Guevara-Carrion, and Jadran Vrabec

Abstract Due to availability of powerful computers and efficient algorithms, physical processes occurring at the micrometer scale can nowadays be studied with atomistic simulations. In the framework of the collaborative research center SFB-TRR75 "Droplet dynamics under extreme ambient conditions", investigations of the mass transport across vapour-liquid interfaces are conducted. Non-equilibrium molecular dynamics simulation is employed to study single- and two-phase shock tube scenarios for a simple noble gas-like fluid. The generated data show an excellent agreement with computational fluid dynamics simulations. Further, particle and energy flux during evaporation are sampled and analysed with respect to their dependence on the interface temperature, employing a newly developed method which ensures a stationary process. In this context, the interface properties between liquid nitrogen and hydrogen under strong gradients of temperature and composition are investigated. Moreover, the Fick diffusion coefficient of strongly diluted species in supercritical CO_2 is predicted by equilibrium molecular dynamics simulation and the Green-Kubo formalism. These results are employed to assess the performance of several predictive equations from the literature.

1 Introduction

Since 1953, molecular modelling and simulation has contributed substantially to thermodynamics and materials science as a numerical approach to investigate the thermophysical behaviour of matter. It is based on the interactions between molecules that are described by force fields and are modeled today on the basis of quantum chemical data. This approach rests on statistical mechanics, which postulates that a macroscopic thermodynamic state in the sense of classical thermodynamics is represented by the sum of its underlying microstates. In other words, when studying a microscopic system by sampling a sufficient number of microstates under appropriate boundary

M. Heinen · S. Homes · G. Guevara-Carrion · J. Vrabec (✉)
Thermodynamics and Process Engineering, Technical University of Berlin, Berlin, Germany
e-mail: vrabec@tu-berlin.de

K. Schulte et al. (eds.), *Droplet Dynamics Under Extreme Ambient Conditions*,
Fluid Mechanics and Its Applications 124,
https://doi.org/10.1007/978-3-031-09008-0_13

conditions, all thermophysical properties of the corresponding macroscopic system can be determined. The accessibility of physical properties with atomistic simulations has been extended by the development of computer hardware and sampling algorithms [4]. For instance, transport properties like the Fick diffusion coefficient matrix of multicomponent mixtures, which are hardly measurable with experiments, can be determined with equilibrium molecular dynamics (EMD).

Due to the fact that the interactions are considered for every molecule individually, the computational effort remains an issue for atomistic simulations. Although the number of calculations can be reduced by considering the interactions only within a certain cutoff radius, the effort is still large, which limits the accessible length and time scales. The length scale is related to the atomic radius of the elements, i.e. a molecular system consisting of a few thousand particles, a typical size for EMD simulations, has an extent of a few nanometers only. The time scale is related to the propagation speed of molecules, which for moderate temperatures is on the order of a few hundred meters per second, depending of the molecular weight. To perform a stable molecular dynamics (MD) simulation, the trajectory of every individual molecule has to be followed with a sufficient temporal resolution. Consequently, a time step on the order of a femtosecond is needed.

Systems consisting of a few hundred molecules, which are small from today's perspective, were a challenge in the past even for the most advanced computers. Due to the exponential growth of computational resources and the development of highly parallelised code [20], however, the accessible length and time scales were significantly extended so that simulations of molecular systems on the micrometer and microsecond scales are feasible today. These orders of magnitude are sufficiently large to obtain results that are directly comparable with computational fluid dynamics (CFD) simulations. Especially due to the limitation of the accessible time scale with atomistic simulations, such direct comparisons with CFD are particularly tractable in situations where rapid physical processes are investigated. This condition was favourable for the research topic of the collaborative research center SFB-TRR75 "Droplet dynamics under extreme ambient conditions". Direct comparisons to models on a coarser level were a central element of the investigations of our group, with the overarching goal to bring insights obtained on the microscopic scale to the macroscopic scale. The aim was to improve the assumptions that have to be made in continuum methods, especially when considering multiphase systems in the presence of interfaces. In the following, a selection of this work is presented, starting with the investigation of single- and two-phase shock tube scenarios, considering a simple noble gas-like fluid in Sect. 2. Next, investigations of stationary evaporation across a planar interface of pure fluids are described in Sect. 3. In Sect. 4, a more complex scenario is discussed, where liquid nitrogen evaporates into a hydrogen gas phase. Finally, selected results on the Fick diffusion coefficient of supercritical fluids are presented in Sect. 5.

2 Shock Tube

The finite volume (FV) scheme is a numerical method for the discretization of the Navier-Stokes equations. Due to its conservative properties, allowing for discontinuities between the grid cells, it is widely used in CFD codes. The flux between grid cells is nowadays determined by the solution of the Riemann problem. This idea was proposed by Godunov in his pioneering work. Since then, the so-called Riemann solvers have been continuously developed so that modern methods reduce the computational effort by approximate solutions, while preserving the advantageous properties of the Godunov scheme.

The most simple example for a Riemann problem is a classical shock tube scenario, consisting of two homogeneous gas phases on different pressure levels that are initially separated by a diaphragm. Once the diaphragm is ruptured, a shock wave is exerted by the high pressure region and propagates through the low pressure region. The Riemann problem solution for this scenario is well known. Hence, it was used as a starting point for the present study, before considering the more challenging case of a two-phase shock tube scenario, where the high pressure gas phase of the classical single-phase shock tube is replaced with a liquid phase and the adjacent gas phase has a pressure below the saturation pressure of the liquid.

The treatment of this case with CFD is much more complex, since the solution structure of the Riemann problem has to be extended accordingly. The solution of the Riemann problem with phase transition, starting from initial data for the interacting phases, must find a path through the two-phase region, wherein the isotherm and isentrope exhibit a Maxwell loop that entails an imaginary speed of sound. This has mathematical consequences in the form that the hyperbolicity of the Euler equations is lost and the partial differential equations become hyperbolic-elliptic. Further implications are discussed in Ref. [12].

Since no analytical solution for the two-phase shock tube exists and open questions with respect to both the modelling and the numerical treatment remain, it was particularly interesting to generate a reference data set with NEMD simulation for this case. The study was divided into two parts. First, two single-phase shock tube scenarios were investigated to assess the general concept of a direct comparison between NEMD and CFD simulations: A classical shock tube scenario with two supercritical gas phases at different pressure levels and the expansion of one supercritical gas phase into vacuum. Second, the more complex case of the two-phase shock tube was investigated. Before selected results are presented in the following, some common features are addressed.

In the according NEMD simulations, a simple molecular model, i.e. the truncated and shifted Lennard-Jones (LJTS) potential, was used. It can be parametrized such that it nicely mimics the thermophysical properties of the noble gases and methane [23]. This model is computationally cheap in MD simulations and two accurate equations of state for its thermophysical properties exist, which were used as an input for the CFD simulations so that both the microscopic (MD) and the macroscopic (CFD) solutions considered exactly the same fluid.

During NEMD simulations, spatially resolved temperature T, density ρ and hydrodynamic velocity v profiles were sampled by employing a classical binning scheme. To capture the dynamics of the shock tube processes, these profiles were averaged over comparatively short time intervals of $\Delta t = 10$ (20 ps for argon) to avoid blurring the rapidly changing profiles. The evolution of these profiles over time was compared to the profiles obtained from CFD simulations. To achieve a good statistical quality despite the short sampling time intervals, comparatively large interface areas were considered by NEMD, yielding configurations comprising a total of up to $3 \cdot 10^8$ particles. Moreover, the statistical quality was raised by a factor of two by exploiting the spatial symmetry of the systems.

The macroscopic CFD solutions were obtained by solving the conservation equations with a discontinuous Galerkin spectral element method (DGSEM) [10], which was implemented in the open source code *FLEXI*[1]. The associated work was done by Munz and coworkers. Detailed comparisons between MD and CFD have recently been published in Refs. [11, 12].

Results for the single-phase shock tube scenario are shown in Fig. 1, covering the well known characteristics of this case, i.e. a shock wave, delimited by a shock front, propagating into the low pressure region, followed by a material boundary with lower propagation speed that initially separated the high and low pressure regions as well as a rarefaction wave that travels in opposite direction into the high pressure region. The comparison between results from MD and CFD simulations showed an almost perfect agreement, which was a good motivation for the consideration of the more complex scenario. Figure 2 shows results for one of the investigated two-phase shock tube scenarios. The snapshots together with the density and velocity profiles illustrate major aspects of the system behaviour. By colouring of the particles and sampling partial density profiles, the spontaneously evaporated matter (red) can be determined.

From the velocity profiles, it can be seen that this matter accelerated the initially resting vapour phase (green) and thereby induced a shock wave. The magnitude of the shock wave, i.e. the compression of the vapour phase, is weak compared to the one observed in the single-phase scenario (note that the left plot of Fig. 2b shows only the range of the vapour density). The shock front and the material boundary, where the latter can be identified at the point where the partial density profiles cross, smear out during their propagation because of diffusion.

A comparison of the results from NEMD and CFD simulations is given in Fig. 3. It clearly shows that the homogeneous equilibrium method simulation failed to reproduce the results from NEMD, whereas results from the sharp interface method show a very good agreement, covering all characteristics of the density, velocity and temperature profiles obtained from NEMD simulation. The temperature profiles, however, revealed that reproducing the evaporative cooling effect by CFD remains an issue. The NEMD results show a much more pronounced temperature drop at the vapour-liquid interface. Consequently, also a deviation for the vapour density close to the liquid phase was found.

[1] https://www.flexi-project.org/.

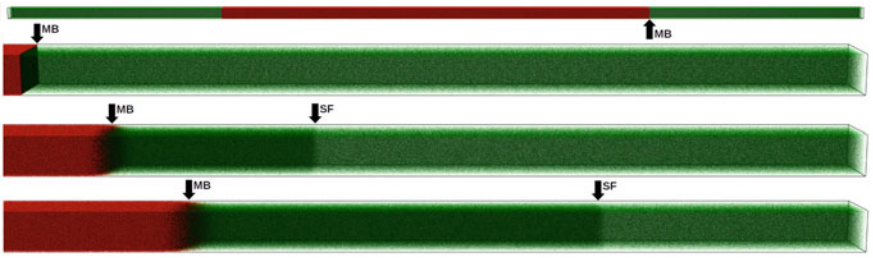

(a)

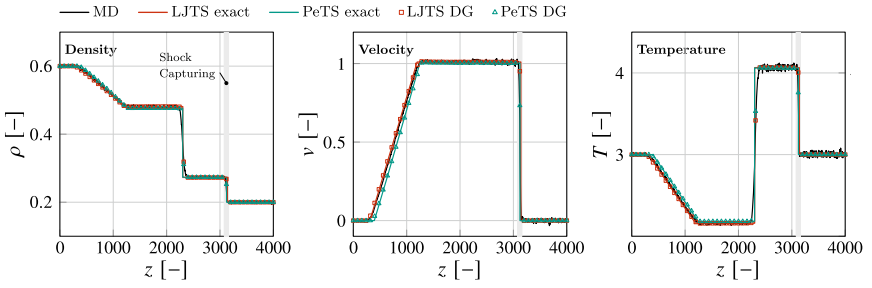

(b)

Fig. 1 Results for the supercritical shock tube problem. **a** Snapshots of the MD system, rendered by *MegaMol* [5], at three instances of time $t = 0$, 182 and 364 with an overall view of the initial configuration (top) followed by magnified views on the right interface and low pressure region. Particles constituting the initial high and low pressure regions are coloured red and green, respectively. Black arrows mark the material boundary (MB) and the shock front (SF). **b** Comparison of the results from MD simulations, the exact solution of the corresponding macroscopic Riemann problem and the approximate solution by the DGSEM scheme. The Riemann problem was solved with the LJTS or the PeTS equation of state. The grey rectangle indicates the region were shock capturing was active [12]

3 Evaporation of a Pure Fluid

To gain further insight into evaporation processes, the evaporative mass transfer of the pure LJTS fluid across a planar vapour-liquid interface was investigated. The focus of the present study [13] laid on the influence of the liquid region. The bulk liquid temperature as well as the thermal resistance were varied and their impact on the evaporation process was analysed by carrying out large NEMD simulations with up to $8.4 \cdot 10^6$ particles using the software *ls1 mardyn* [20].

A common method to investigate evaporation processes harnesses a symmetrical molecular system. Such a system consists of two vapour phases surrounding a liquid phase, cf. Fig. 4a. Besides imposing periodic boundary conditions at the volume faces that are perpendicular to the interface, a vacuum is used to enforce a driving gradient for evaporation. Since particles are deleted in the vacuum region, the total number of particles in the system decreases, leading to a receding interface, which entails

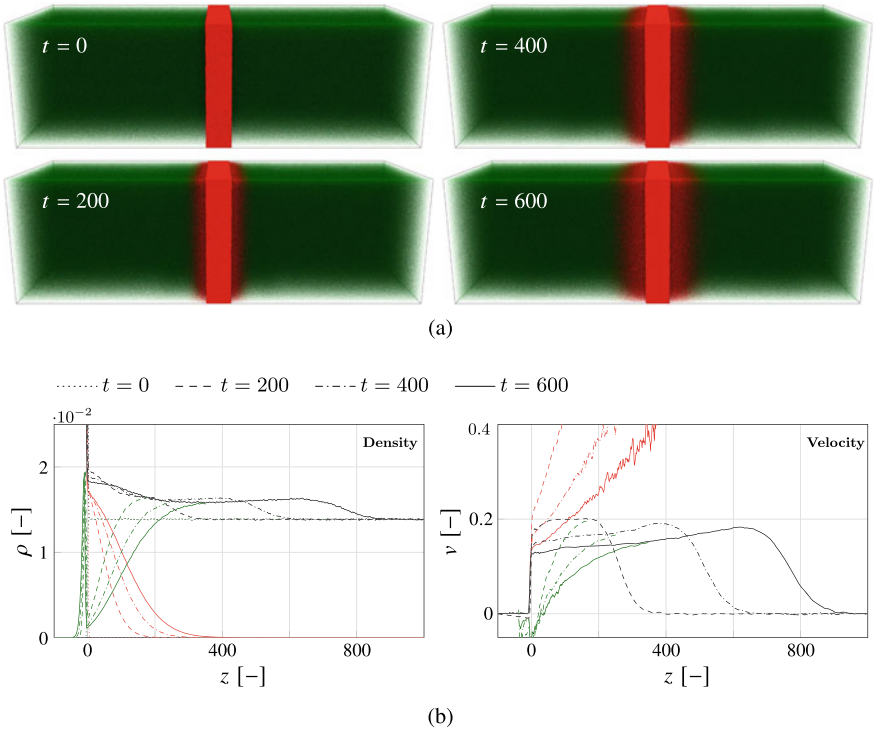

Fig. 2 Results for a two-phase shock tube scenario obtained from NEMD simulation. **a** Snapshots [5] of the MD system at four instances of time $t = 0$, 200, 400 and 600. Particles that were initially constituting the liquid and vapour phase are coloured red and green, respectively. **b** Evolution of density ρ and hydrodynamic velocity v profiles depicted at the same time instances as the snapshots. Partial density and partial velocity profiles were sampled considering only particles that were initially constituting the liquid (red) or the vapour phase (green), respectively. The total density and velocity profiles (black) are the weighted sum of the partial ones

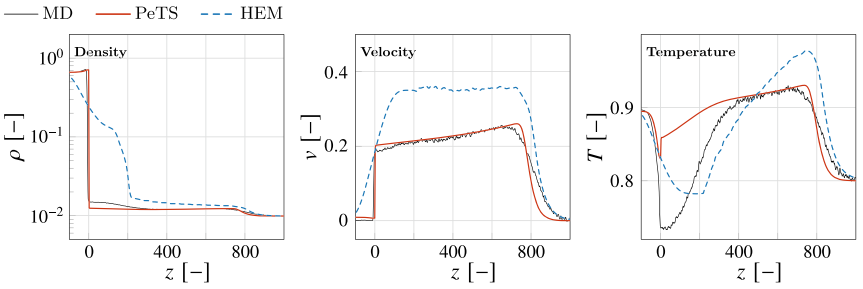

Fig. 3 Density ρ, velocity v and temperature T profiles at time $t = 600$ obtained from NEMD and CFD simulations with both approaches, the sharp interface method (PeTS) and the homogeneous equilibrium method (HEM). The initial conditions of the depicted case refer to the strongest non-equilibrium considered in Ref. [12]

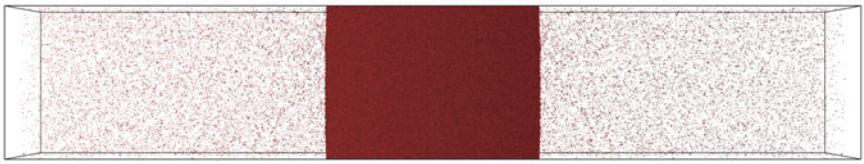

(a)

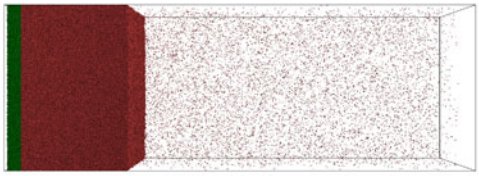

(b)

Fig. 4 Snapshots [5] of systems for the investigation of evaporation. **a** Symmetrical method with two vapour and one liquid phase as it is commonly used. **b** Present method to maintain stationary conditions

several disadvantages. The receding interface allows only for a limited sampling duration, since the liquid phase vanishes at some point in time. Moreover, it is not possible to simulate very large systems because they require a long time to reach quasi-stationarity.

In order to overcome these challenges, our collaborating partner Müller-Plathe and coworkers [31] developed two methods to simulate stationary evaporation, which are based on sophisticated algorithms for particle insertions to replenish the liquid. They showed that those algorithms could be used successfully in situations with high evaporation rates and also for more complex molecules such as ethanol. To guarantee smooth insertions, however, a few control parameters have to be specified in a careful manner. Hence, for the specific case of stationary evaporation across a planar interface a new method was developed that works without the need of any parameters [9]. As shown in Fig. 4b, the system is constituted by one liquid and one vapour phase. There is still a vacuum on the right-hand side, where particles are deleted, but in contrast to the common method, these are replaced by a slab of liquid that is pushed into the system at its left boundary. Hence, the total number of particles within the system remains constant. Since the liquid slab is continuously replenished, stationary conditions are guaranteed, facilitating arbitrarily long simulation runs.

This method is suited for the present parameter study, since systems with a large number of particles were investigated. Besides the vacuum at the right boundary, a thermostat in the bulk liquid constrained the system. In that thermostated region, the velocity of the particles was scaled such that a specified bulk liquid temperature T_{liq} was maintained. The second quantity which was varied in this study was the distance L_{n} between the thermostat and the interface. After reaching stationary conditions, all desired quantities, like density, temperature and velocity profiles, were sampled

for about 10^6 time steps. The sampling was performed in bins with a width of 1/4 particle diameters. Further details on the methodology can be found in Ref. [13].

A stationary simulation is characterised by several quantities. The present study focused on the particle flux j_p and energy flux j_e that are constant over the simulation volume under stationary conditions. Both fluxes were not sampled directly, but calculated during post-processing. Quantities which were sampled directly include the hydrodynamic velocity v_z, density ρ and temperature T. Those profiles were combined as follows to yield the particle flux j_p

$$j_\mathrm{p} = \rho v_z.$$

While the particle flux rises with increasing bulk liquid temperature, it decreases for a larger distance between the thermostated region and the interface L_n. Furthermore, an asymptotic behaviour was observed, as the particle flux reaches a certain value j_p^∞ for a distance L_n extrapolated to infinity.

In analogy with the particle flux, the energy flux j_e was calculated by post-processing using the directly sampled profiles. The following equation was used

$$j_\mathrm{e} = (h + e_\mathrm{kin}) j_\mathrm{p} + \dot{q},$$

in which h is the enthalpy, e_kin the kinetic energy and $\dot{q}$ the heat flux. In order to obtain the enthalpy h, an equation of state [8] was utilised to compute the enthalpy as a function of temperature and density. The kinetic energy e_kin was derived straightforwardly from the directly-sampled hydrodynamic velocity. The heat flux $\dot{q}$ was determined with Fourier's law for which the thermal conductivity was taken from two correlations [15, 16] and the directly sampled temperature and density profiles as input parameters.

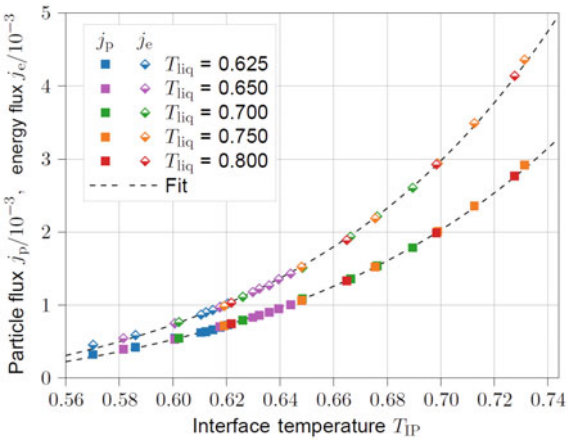

Fig. 5 Particle flux j_p and energy flux j_e over the interface temperature T_IP for all conducted simulations

Similar to the fluxes, the interface temperature T_{IP} depends on the bulk liquid temperature T_{liq} as well as on the distance between thermostat and interface L_{n}. Nevertheless, when investigating the dependence of the fluxes on the interface temperature, it turns out that both the particle flux and the energy flux depend under the given boundary conditions solely on the interface temperature, cf. Fig. 5. Regardless of the initial parameters, like bulk liquid temperature and distance between thermostat and interface, simulations yield the same fluxes when their interface temperature is the same. Under the present boundary conditions, this holds for the entire investigated temperature range.

4 Evaporation of Liquid Nitrogen into Hydrogen

The injection process in liquid propellant rocket engines is a prominent example of extreme conditions, which are characterised by high pressures and cryogenic injection temperatures. While the chamber pressure often exceeds the critical pressure of the injected fluid, the injection temperature of one or both propellants is usually below or close to the critical temperature of the pure fluid so that they are in a trans- or supercritical state. Especially due to the high operating pressure, the experimental conditions are very challenging and therefore the process-relevant quantities are difficult to access metrologically. Moreover, a better understanding of the atomisation process is of great scientific and also economic interest due to the savings potential through possible optimisations.

An early experimental work on this topic was carried out by Oschwald et al. [22], where coaxial injection processes of liquid nitrogen (LN_2) into gaseous hydrogen (H_2) at supercritical pressure were studied with Raman scattering. Nitrogen was used as a substitute for oxygen in order to allow for an isolated observation of the mixing processes with the exclusion of chemical reactions. Avoiding experimental challenges, Müller et al. [19] investigated two of the test cases (D4 and E4) of Ref. [22] with large-eddy simulations. For the transcritical injection conditions (E4), the simulation results showed that thermodynamic states occur in the shear layer that lie in the two-phase region, as indicated by a vapour-liquid equilibrium calculation. These results, however, contradicted the findings of Dahms and Oefelein [3], who proposed a model to predict the operating pressure where classical sprays transition to dense-fluid mixing, based on a Knudsen number criterion using the interface thickness as the representative physical length scale. While a lively discussion on this topic continued in the rocket combustion community, Traxinger et al. [28] extended the thermodynamic framework used in Ref. [19] to additionally account for multicomponent phase separation by means of a vapour-liquid equilibrium model. Employing this extended framework for the case of n-hexane injected into a chamber containing nitrogen in a combined experimental and numerical study, results from both were in good agreement, showing phase separation and the transition from a dense-gas to a spray-like jet for the test cases where the a priori calculation predicted a two-phase flow.

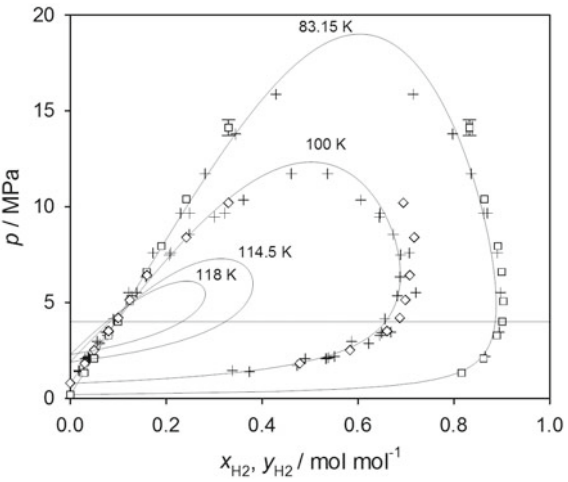

Fig. 6 Isothermal phase diagram of the binary mixture $H_2 + N_2$ obtained by molecular simulation (squares and diamonds), Peng-Robinson equation of state (solid lines) and experiment (crosses) [14]. The horizontal line marks the pressure $p = 4$ MPa of the low pressure case NEMD simulation

Contributing to the understanding of such processes, three NEMD simulations were conducted in the present study, investigating a LN_2/H_2 interface exposed to strong temperature and composition gradients, considering similar conditions as test case E4 of Ref. [22]. The force fields selected to model the molecular interactions of hydrogen and nitrogen have shown their validity in a prior study where the phase behaviour of this binary mixture was investigated by EMD simulations, cf. Fig. 6.

While maintaining the same temperature and composition gradient for all three NEMD simulations, the system pressure was varied $p = 4$, 12 and 20 MPa. Since the two highest pressures showed qualitatively similar results, the terms '*low pressure case*' ($p = 4$ MPa) and '*high pressure case*' ($p = 12$ or 20 MPa) are used in the following. Figure 7a shows a snapshot of the system's initial configuration in the low pressure case, consisting of two homogeneous and pure phases (LN_2 and H_2) in physical contact through a comparatively large planar interface with an area of $(85\,\text{nm})^2$ to obtain sampling results with a high statistical quality. Hence, a configuration comprised a total of $\sim 10^7$ molecules. The LN_2 and H_2 phases had a width of 50 nm and 140 nm, respectively, yielding an overall extent of the system of 190 nm in z direction.

Before these phases were brought into contact, they were both thoroughly equilibrated by EMD simulation in the canonic ensemble. The liquid slab of LN_2 had a temperature of $T_{N2} = 118$ K and the H_2 gas phase had a temperature of $T_{H2} = 270$ K. Once the initial configurations were prepared, NEMD simulations were conducted to follow the temporal evolution of the system, in particular the vapour-liquid interface. During these simulations, the state of the bulk phases LN_2 and H_2 was controlled within control volumes (CV) at the outer limits of the system in z direction, cf. Fig. 7a. In both CV, the composition was controlled to maintain the fluids in their pure state. This was achieved by identity change, i.e. hydrogen molecules entering the CV in the liquid phase were substituted by nitrogen molecules and nitrogen molecules entering

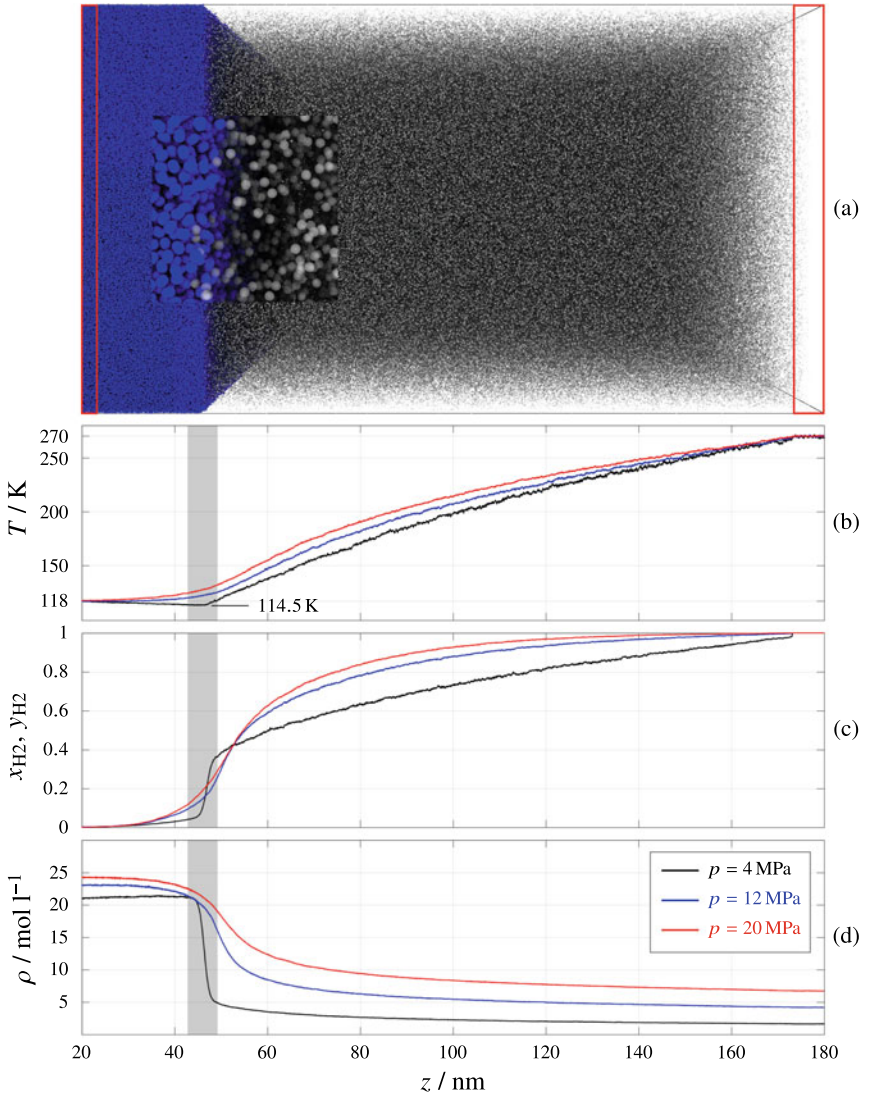

Fig. 7 **a** Snapshot [5] of the initial configuration of the low pressure case ($p = 4$ MPa), consisting of a liquid nitrogen LN_2 phase at a temperature of $T_{N2} = 118$ K on the left and a supercritical hydrogen H_2 phase at a temperature of $T_{H2} = 270$ K on the right side. The inset shows a magnified view on the interface. Two control volumes (CV), in which the boundary conditions in z direction were maintained, are marked by red rectangles. Temperature T, mole fraction of hydrogen x_{H2}, y_{H2} and density ρ profiles are shown in panels **b–d** for the three pressure cases: $p = 4$ MPa (black), $p = 12$ MPa (blue) and $p = 20$ MPa (red). The grey area marks the interface region of the low pressure case

the CV in the gas phase were substituted by hydrogen molecules. The temperatures $T_{N2} = 118\,K$ and $T_{H2} = 270\,K$ were controlled in the CV by velocity scaling. Moreover, the desired system pressure was maintained indirectly by imposing a constant density within the gas phase CV by particle deletion. Finally, the liquid phase was replenished from a liquid reservoir to maintain stationary conditions, cf. Ref. [9].

To investigate the system behaviour, the temperature T, hydrogen mole fraction x_{H2}, y_{H2} and density ρ profiles were sampled by NEMD simulation employing a classical binning scheme. Because of the strong thermodynamic non-equilibrium between the two phases in the initial configuration, a rapid transition from the stepwise profiles to the profiles under stationary conditions was observed, cf. Fig. 7b–d. These were attained after a time period of approximately 3 ns in all pressure cases. One of the striking features of the density profiles is that with increasing pressure not only the gas density of the H_2 bulk phase increased (almost linearly), but also the density of the LN_2 phase increased, indicating a compressible liquid. However, this is not surprising since $T_{N2} = 118\,K$ is close to the critical temperature of nitrogen $T_{c,N2} = 126\,K$. Considering the transition from liquid to gas, a clear difference between the pressure cases can be noticed. In the low pressure case, a sharp interface with a thickness of only a few nanometers was observed, whereas the high pressure cases show much broader and comparatively smooth transitions that span over tens of nanometers, which can be identified as dense-fluid mixing. A similar observation was made for the mole fraction profile x_{H2}, y_{H2}. The low pressure case shows a steep gradient at the interface, which can be interpreted as a resistance for hydrogen to dissolve into the LN_2 phase, whereas the higher pressure cases show much broader and comparatively smooth transitions, similar to the density profile. The temperature profiles exhibit an overall similar course. However, a particular characteristic was revealed at the interface. In the low pressure case, a temperature decrease towards the interface was observed, leading to a minimum of 114.5 K. This means that despite a much higher temperature of the gas phase, a part of the enthalpy of evaporation was supplied by the liquid phase. Conversely, in the high pressure cases, the liquid phase was heated up, despite the evaporative cooling effect. This can be explained by the much more intense thermal coupling between the liquid and gas phase at higher pressure, predominantly due to the higher gas density.

To further asses these results, they were compared to an isothermal phase diagram of the binary mixture $H_2 + N_2$ [14], cf. Fig. 6. The diagram shows the vapour pressure over the hydrogen mole fraction x_{H2}, y_{H2} for four isotherms. Since the critical temperature of hydrogen is $T_{c,H2} = 33\,K$, all isotherms are tied up to the vapour pressure of pure nitrogen only. With increasing temperature, the two-phase region becomes much smaller and recedes toward pure nitrogen so that at a certain temperature limit the mixture is found to be supercritical at any pressure and composition. Considering a pressure of $p = 4\,MPa$ (low pressure case), a stable vapour-liquid equilibrium can be found for all depicted isotherms, where with decreasing temperature the critical point of the mixture becomes more distant to the 4 MPa line. That means that the evaporative cooling effect, leading to a decreased interface temperature of 114.5 K, stabilises the presence of the interface when assuming local equilibrium conditions. Conversely, the increased interface temperature due to enhanced thermal coupling of

the liquid and gas phase, as observed in the NEMD simulations of the high pressure cases, leads to a reduced critical pressure of the mixture and thereby to a weakened interface.

5 Diffusion in the Supercritical Region

Diffusion is one of the key processes in the context of mass transfer across interfaces. For instance, evaporation of liquids into a vapour phase driven by a chemical potential gradient is often rate-limited by diffusion [2]. Mass transport of one component in the presence of a stagnant gas, known as Stefan diffusion, often occurs during adsorption and condensation operations [27]. Analyses of evaporation experiments in a Stefan tube require the Fick diffusion coefficient near the infinite dilution limit, since the evaporating species is present in extremely low concentrations at the top of the tube. Therefore, it is important to identify adequate procedures to obtain reliable diffusion coefficient data under these conditions.

This work focuses on the prediction of the Fick diffusion coefficient of various solutes diluted in supercritical carbon dioxide (CO_2), which is an environmentally friendly solvent employed in various industrial processes [21]. The measurement of diffusion coefficients in supercritical CO_2 is experimentally challenging and many techniques still require improvement to reach an adequate accuracy. Data availability is thus limited, especially in the extended critical region. Driven by the lack of experimental data, many models and correlations, mainly based on the Stokes-Einstein equation or the rough-hard-sphere model, have been developed to predict the Fick diffusion coefficient. An overview of the proposed predictive equations with their strengths and shortcomings can be found in recent reviews [17, 26].

On the other hand, EMD simulation offers a physically sound route not only to predict diffusion data, but also to gain an insight into the underlying molecular mechanisms. Therefore, EMD simulation and the Green-Kubo formalism were employed here to predict Fick diffusion coefficients of methane (CH_4), benzene (C_6H_6) and toluene (C_7H_8) diluted in supercritical CO_2 under near-critical conditions. The simulation results were subsequently compared with several predictive equations from the literature.

Rigid, non-polarizable, Lennard-Jones (LJ) based force fields were chosen. If required, superimposed point quadrupoles were used to account for the electrostatic interactions. The description of the force fields and the corresponding parameters can be found in Refs. [6, 18, 29]. To specify the unlike interactions between LJ sites, a modification of the Lorentz-Berthelot combining rules given by $\sigma_{ab} = (\sigma_{aa} + \sigma_{bb})/2$ and $\epsilon_{ab} = \xi\sqrt{\epsilon_{aa}\epsilon_{bb}}$, was employed. The parameter ξ was obtained by adjusting the sampled vapour-liquid equilibrium to experimental data for each binary mixture.

One way to obtain the Fick diffusion coefficient D_{ij} is to calculate it from the sampled Maxwell-Stefan (MS) diffusion coefficient $Đ_{ij}$ employing the relation

$$D_{ij} = Đ_{ij} \cdot \Gamma \,, \tag{1}$$

where Γ is the so-called thermodynamic factor, which is given by

$$\Gamma = \frac{x_1}{k_B T} \left(\frac{\partial \mu_1}{\partial x_1} \right)_{T,p} . \tag{2}$$

Therein, x_1 and μ_1 are the mole fraction and the chemical potential of component 1, respectively, and k_B is the Boltzmann constant.

The thermodynamic factor is usually obtained from an equation of state or an excess Gibbs energy model fitted to experimental phase equilibrium data. However, it can also be estimated by molecular simulation, either by sampling the chemical potential or Kirkwood-Buff integrals. In this work, the chemical potential was sampled with Widom's test particle method and the right-hand side of Eq. (2) was then approximated by numerical differentiation.

The thermodynamic factor is defined to be unity at the infinite dilution limit where both MS and Fick diffusion coefficients are equivalent. In the case of dense liquids, the thermodynamic factor is usually approximated by unity near the infinite dilution limit. However, in the extended critical region, the thermodynamic factor can largely differ from unity even for strongly diluted mixtures.

Intra-, MS and Fick diffusion coefficients of methane, benzene and toluene diluted in supercritical CO_2 were sampled in the temperature range between 295 and 335 K along the isobar p = 9 MPa. The corresponding equations have been reported previously, e.g. in Ref. [6], and are not repeated here. Figure 8 shows the temperature dependence of the different diffusion coefficients predicted for the three diluted mixtures with a CO_2 mole fraction of x_{CO2} = 0.99 mol·mol^{-1}. The MS diffusion coefficient predicted with Darken's equation is also shown. As expected, the intra-diffusion coefficient of CO_2 is lower than that of methane and higher than that of benzene and toluene because of the differing molecular mass. Further, Darken's equation is consistent with the predicted MS diffusion coefficient for all regarded mixtures, which suggests the presence of rather unspecific intramolecular interactions between unlike species. In general, the diffusion coefficients increase with temperature. Note that between 308 and 320 K, intra- and MS diffusion coefficients show a significant step-wise variation with temperature, which is related to the likewise strong change of the mixtures' density in this temperature range.

On the other hand, the Fick diffusion coefficient shows a different behaviour, which can be clearly observed for the mixtures with benzene and toluene, cf. Fig. 8. An anomalous decrease of the Fick diffusion coefficient with rising temperature was found, which can be explained on the basis of Eq. (1). The Fick diffusion coefficient consists of two contributions, the hydrodynamic represented by the MS diffusion coefficient $Đ_{ij}$ and the thermodynamic contribution given by Γ. Although the MS diffusion coefficient increases strongly with temperature, the thermodynamic factor reaches values far below unity due to the proximity of the critical point. The combination of both effects yields the observed behaviour of the Fick diffusion coefficient.

A number of different expressions to predict the temperature dependence of the Fick diffusion coefficient for strongly diluted binary mixtures is available in the

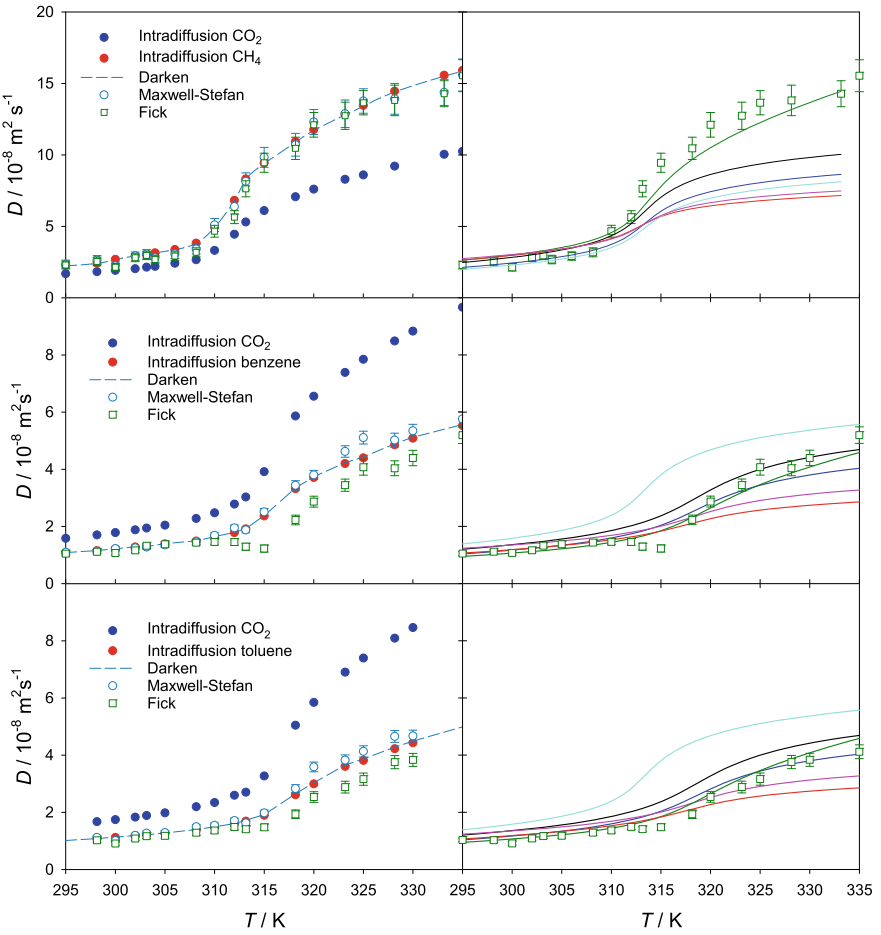

Fig. 8 (left) Temperature dependence of the intra-, Maxwell-Stefan and Fick diffusion coefficients for the mixtures (top) $CH_4 + CO_2$, (center) $C_6H_6 + CO_2$ and (bottom) $C_7H_8 + CO_2$ at $p = 9$ MPa and $x_{CO2} = 0.99$ mol mol^{-1}. (right) Simulation results for the Fick diffusion coefficient (green squares) are compared with predictive equations (lines) by Sassiat et al. [24] (black), Wilke and Chang [30] (blue), Catchpole and King [1] (green), He and Yu [7] (red) and Scheibel [25] (cyan)

literature, many of which were developed exclusively for supercritical CO_2 mixtures. Figure 8 shows the predicted Fick diffusion coefficient for the studied mixtures employing the equations by Sassiat et al. [24], Scheibel [25], Wilke and Chang [30], Catchpole and King [1] as well as He and Yu [7]. Further equations are not shown for the sake of clarity. As can be seen, these equations yield significantly different values for the Fick diffusion coefficient at temperatures above 315 K. Generally, the equation proposed by Catchpole and King [1] yields the best agreement with present simulation results for all mixtures in the regarded temperature range. Other predictive equations show an acceptable agreement with simulation only for temperatures below

315 K, e.g. the well-known Wilke-Chang equation [30]. In general, it was observed that the predictive equations which explicitly include the solvent density perform better. However, it is clear that a trustworthy equation to predict the Fick diffusion coefficient under conditions regarded in this work is still to be developed.

6 Conclusions

With the overarching goal of transferring insight from the microscopic to the macroscopic scale, different studies were conducted by atomistic simulations to investigate mass transport across vapour-liquid interfaces under various conditions related to engineering applications.

Classical single-phase and two-phase shock tube scenarios were investigated using a model fluid (LJTS). As a reference data set, results of NEMD simulations were compared with those obtained from CFD simulations, for which the collaborating partner Munz and coworkers developed a new Riemann solver. By means of an accurate equation of state for the LJTS fluid as input for the CFD simulations, a direct comparison with the NEMD results became feasible. It showed an excellent agreement for the single-phase shock tube scenario and also very good agreement for the much more complex two-phase shock tube scenario.

The LJTS fluid was considered again for the investigation of the evaporation process across a planar interface. With a newly developed method, which allows to maintain stationary conditions for an arbitrarily long simulation time, it was possible to study large systems of up to $8.4 \cdot 10^6$ particles of the LJTS fluid. Quantities like the hydrodynamic velocity, temperature and density were sampled directly and used to calculate further properties like the particle flux and the energy flux. Under the given boundary conditions, it was shown that both fluxes solely depend on the interface temperature.

The evaporation process across a planar interface was also studied for a more complex case, i.e. the binary mixture of liquid nitrogen and gaseous hydrogen. The conditions in the bulk phases were specified to correspond to the extreme conditions encountered in liquid propellant rocket engines, i.e. with strong temperature and composition gradients across the interface. The study focused on the question, under which conditions the atomisation process transitions from a classical spray to dense-fluid mixing. For this purpose, NEMD simulations were performed at three different pressure levels. At the lowest pressure level, the interface remained stable, whereas at the higher pressure levels, diffuse mixing was observed.

A detailed description of diffusion is important for the study of evaporation processes. Intra-, Maxwell-Stefan and Fick diffusion coefficients of methane, benzene and toluene diluted in supercritical carbon dioxide were predicted by equilibrium molecular dynamics simulation and the Green-Kubo formalism. Under near-critical conditions, it was observed that the Fick diffusion coefficient exhibits an anomalous behaviour, which was explained by the decrease of the thermodynamic factor. Further, several predictive equations for the Fick diffusion coefficient were compared

with present simulation results. Although some equations were able to reasonably predict the temperature dependence of the Fick diffusion coefficient at the studied conditions, none of the studied equations could be established as reliable.

Acknowledgements The authors kindly acknowledge the financial support by the Deutsche Forschungsgemeinschaft (DFG) within the SFB-TRR 75, project number 84292822. The simulations were performed on the national supercomputer HPE Apollo (Hawk) at the High Performance Computing Center Stuttgart (HLRS) as well as on the cluster Cray CS500 (Noctua) at the Paderborn Center for Parallel Computing (PC^2) and the supercomputer SuperMUC-NG at the Leibniz Supercomputing Centre Garching (LRZ).

References

1. Catchpole OJ, King MB (1994) Measurement and correlation of binary diffusion coefficients in near critical fluids. Ind Eng Chem Res 33:1828–1837
2. Chatwell RS, Heinen M, Vrabec J (2019) Diffusion limited evaporation of a binary liquid film. Int J Heat Mass Transf 132:1296–1305
3. Dahms RN, Oefelein JC (2015) Atomization and dense-fluid breakup regimes in liquid rocket engines. J Propuls Power 31:1221–1231
4. Fingerhut R, Guevara-Carrion G, Nitzke I, Saric D, Marx J, Langenbach K, Prokopev S, Celný D, Bernreuther M, Stephan S, Kohns M, Hasse H, Vrabec J (2021) ms2: a molecular simulation tool for thermodynamic properties, release 4.0. Comput Phys Commun 262:107860
5. Grottel S, Krone M, Muller C, Reina G, Ertl T (2015) MegaMol—a prototyping framework for particle-based visualization. IEEE Trans Vis Comput Graph 21:201–214
6. Guevara-Carrion G, Janzen T, Munoz-Munoz YM, Vrabec J (2016) Mutual diffusion of binary liquid mixtures containing methanol, ethanol, acetone, benzene, cyclohexane, toluene, and carbon tetrachloride. J Chem Phys 144:124501
7. He CH, Yu YS (1998) New equation for infinite-dilution diffusion coefficients in supercritical and high-temperature liquid solvents. Ind Eng Chem Res 37:3793–3798
8. Heier M, Stephan S, Liu J, Chapman WG, Hasse H, Langenbach K (2018) Equation of state for the Lennard-Jones truncated and shifted fluid with a cut-off radius of 2.5 sigma based on perturbation theory and its applications to interfacial thermodynamics. Mol Phys 116:2083–2094
9. Heinen M, Vrabec J (2019) Evaporation sampled by stationary molecular dynamics simulation. J Chem Phys 151:044704
10. Hindenlang F, Gassner GJ, Altmann C, Beck A, Staudenmaier M, Munz CD (2012) Explicit discontinuous Galerkin methods for unsteady problems. Comput Fluids 61:86–93
11. Hitz T, Heinen M, Vrabec J, Munz CD (2020) Comparison of macro- and microscopic solutions of the Riemann problem I. Supercritical shock tube and expansion into vacuum. J Comput Phys 402:109077
12. Hitz T, JÃüns S, Heinen M, Vrabec J, Munz CD (2021) Comparison of macro- and microscopic solutions of the Riemann problem II. Two-phase shock tube. J Comput Phys 429:110027
13. Homes S, Heinen M, Vrabec J, Fischer J (2021) Evaporation driven by conductive heat transport. Mol Phys 119(15–16):e1836410
14. Köster A, Thol M, Vrabec J (2018) Molecular models for the hydrogen age: hydrogen, nitrogen, oxygen, argon, and water. J Chem Eng Data 63:305–320
15. Lautenschlaeger MP, Hasse H (2019) Transport properties of the Lennard-Jones truncated and shifted fluid from non-equilibrium molecular dynamics simulations. Fluid Phase Equilib 482:38–47
16. Lemmon EW, Jacobsen RT (2004) Viscosity and thermal conductivity equations for nitrogen, oxygen, argon, and air. Int J Thermophys 25:21–69

17. Medina I (2012) Determination of diffusion coefficients for supercritical fluids. J Chromatogr A 1250:124–140
18. Merker T, Engin C, Vrabec J, Hasse H (2010) Molecular model for carbon dioxide optimised to vapour-liquid equilibria. J Chem Phys 132:34512
19. Müller H, Pfitzner M, Matheis J, Hickel S (2016) Large-eddy simulation of coaxial LN2/GH2 injection at trans- and supercritical conditions. J Propuls Power 32:46–56
20. Niethammer C, Becker S, Bernreuther M, Buchholz M, Eckhardt W, Heinecke A, Werth S, Bungartz HJ, Glass CW, Hasse H, Vrabec J, Horsch M (2014) ls1 mardyn: The massively parallel molecular dynamics code for large systems. J Chem Theory Comput 10:4455–4464
21. Nikolai P, Rabiyat B, Aslan A, Ilmutdin A (2019) Supercritical CO2: properties and technological applications—a review. J Thermal Sci 28:394–430
22. Oschwald M, Schik A, Klar M, Mayer W (1999) Investigation of coaxial LN2/GH2-injection at supercritical pressure by spontaneous raman scattering. In: 35th joint propulsion conference and exhibit
23. Rutkai G, Thol M, Span R, Vrabec J (2016) How well does the Lennard-Jones potential represent the thermodynamic properties of noble gases? Mol Phys 115:1104–1121
24. Sassiat PR, Mourier P, Caude MH, Rosset RH (1987) Measurement of diffusion coefficients in supercritical carbon dioxide and correlation with the equation of Wilke and Chang. Anal Chem 59:1164–1170
25. Scheibel EG (1954) Liquid diffusivities. Ind Eng Chem 46:2007–2008
26. Suarez JJ, Medina I, Bueno JL (1998) Diffusion coefficients in supercritical fluids: available data and graphical correlations. Fluid Phase Equilib 153:167–212
27. Taylor R, Krishna R (1993) Multicomponent mass transfer. Wiley, New York
28. Traxinger C, Pfitzner M, Baab S, Lamanna G, Weigand B (2019) Experimental and numerical investigation of phase separation due to multicomponent mixing at high-pressure conditions. Phys Rev Fluids 4:074303
29. Vrabec J, Stoll J, Hasse H (2001) A set of molecular models for symmetric quadrupolar fluids. J Phys Chem B 105:12126–12133
30. Wilke CR, Chang P (1955) Correlation of diffusion coefficients in dilute solutions. AIChE J 1:264–270
31. Zhang J, Müller-Plathe F, Yahia-Ouahmed M, Leroy F (2013) A steady-state non-equilibrium molecular dynamics approach for the study of evaporation processes. J Chem Phys 139:134701